Self-Association of the Yeast Nucleosome Assembly Protein 1

Steven J. McBryant and Olve B. Peersen*

Department of Biochemistry and Molecular Biology, Colorado State University, Fort Collins, Colorado 80523-1870

Received October 20, 2003; Revised Manuscript Received May 7, 2004

ABSTRACT: The self-association properties of the yeast nucleosome assembly protein 1 (yNAP1) have been investigated using biochemical and biophysical methods. Protein cross-linking and calibrated gel filtration chromatography of yNAP1 indicate the protein exists as a complex mixture of species at physiologic ionic strength (75−150 mM). Sedimentation velocity reveals a distribution of species of 4.5−12 Svedbergs (S) over a 50-fold range of concentrations. The solution-state complexity is reduced at higher ionic strength, allowing for examination of the fundamental oligomer. Sedimentation equilibrium of a homogeneous 4.5 S population at 500 mM sodium chloride reveals these species to be yNAP1 dimers. These dimers self-associate to form higher order oligomers at more moderate ionic strength. Titration of guanidine hydrochloride converts the higher order oligomers to the homogeneous 4.5 S dimer and then converts the 4.5 S dimers to 2.5 S monomers. Circular dichroism shows that guanidine-mediated dissociation of higher order oligomers into yNAP1 dimers is accompanied by only slight changes in secondary structure. Dissociation of the dimer requires a nearly complete denaturation event.

The nucleosome is a large nucleoprotein assembly containing a minimum of 146 bp of DNA and an octamer of histone proteins composed of a central $(H3-H4)_2$ tetramer flanked on either side by two H2A−H2B dimers (*1*, *2*). The positions of these histone subcomplexes within the nucleosome mandate that the tetramer be deposited on the DNA first, followed by the two dimers (*3*, *4*). Consistent with this, kinetic studies have determined that the H2A−H2B dimer exchanges rapidly in nuclear chromatin, while the $(H3-H4)_2$ tetramer is very stably associated with DNA (*5*). The ordered assembly of nucleosomes is mediated by a large and often redundant family of proteins known as histone chaperones or chromatin assembly factors (reviewed in refs *6* and *7*). These factors are generally acidic in nature and serve to deposit the basic histone proteins onto the newly synthesized DNA. Members of this family include the *Xenopus* factor nucleoplasmin (Np) and its *Drosophila* homologue dNLP, *Xenopus* N1/N2, and the ubiquitous NAP-type histone chaperones (*3*, *8*). Although no obvious sequence homology exists between the nucleoplasmin/NLP1 and NAP-type chaperones, functional similarities have led them to be grouped together within the histone chaperone family.

The nucleosome assembly protein 1 (NAP1) has been well studied with regard to its nucleosome assembly activity (*9*−*11*) and its histone-binding ability (*12*, *13*). NAP1 can also remove an H2A−H2B dimer from a nucleosomal array (*14*). *Saccharomyces cerevisiae* NAP1 (yNAP1)[1] is a 48 kDa protein that is highly acidic with a calculated pI of 4.23 due to 24% aspartic and glutamic acid content. Though considered an H2A−H2B histone chaperone, recent evidence suggests that yNAP1 has a higher affinity for the $(H3-H4)_2$ tetramer (*12*). Analysis of the stoichiometry of the complexes formed between yNAP1 and histones indicates that two yNAP1 molecules bind an H2A−H2B dimer and four bind a $(H3-H4)_2$ tetramer. Furthermore, multiple histone-containing yNAP1 bands were observed in native PAGE assays, suggesting that yNAP1 might exist in more than one functional oligomeric form (*12*).

Little is known about the solution structure of NAP1 or how it may relate to histone binding and chromatin assembly functions. yNAP1 has been reported to sediment at an unexpectedly high molecular weight in sucrose gradients (*11*), and *Drosophila* NAP1 elutes from a gel filtration column with an apparent molecular mass of 600 kDa (*9*). However, it has also been reported that yNAP1 fails to form cross-linked oligomers in the presence of disuccinimidyl suberate, suggesting yNAP1 is monomeric (*13*). It has also been reported that the chaperones Np (*15*) and NLP1 (*16*) self-associate and that self-association is intimately linked to histone binding (*17*). We hypothesized that self-association may be a general property of these histone-binding proteins, though no comprehensive study of a NAP-type chaperone has been reported.

In this study, protein cross-linking, gel filtration chromatography (GFC), analytical ultracentrifugation (AUC), and circular dichroism (CD) spectroscopy are used to examine the self-association properties of yNAP1 in solution. We show that yNAP1 is a stable dimer and that this dimer self-associates in a complex, concentration- and salt-dependent fashion. A moderate concentration of chaotrope was sufficient to dissociate the stable dimer, and this is accompanied by a significant loss of secondary structure that results in a denatured monomer. The implications of yNAP1 oligomerization in terms of histone binding and nucleosome assembly are discussed.

* To whom correspondence should be addressed. E-mail: Olve.Peersen@ColoState.edu.

[1] Abbreviations: AUC, analytical ultracentrifugation; CD, circular dichroism; DiMes, dimethyl suberimidate; GFC, gel filtration chromatography; MALDI-TOF, matrix-assisted laser desorption ionization time-of-flight; rms, root mean square; SE, sedimentation equilibrium; SV, sedimentation velocity; yNAP1, yeast nucleosome assembly protein 1.

10.1021/bi035881b CCC: $27.50
Published on Web 07/23/2004

EXPERIMENTAL PROCEDURES

Reagents and Buffers. All buffers and solutions were made with reagent grade chemicals and distilled, deionized water. Analytical ultracentrifugation (AUC) buffers contained 20 mM sodium phosphate, pH 7.6, 1 mM dithiothreitol (DTT), and the indicated amount of sodium chloride (NaCl). Chromatography buffers contained 20 mM Tris−HCl, pH 7.6 (4 °C), NaCl at the indicated concentration, 10% glycerol, 1 mM DTT, and 0.1 mM PMSF, except for gel filtration experiments, where PMSF was omitted. Solutions were sterile filtered prior to use.

Protein Purification and Handling. The N-terminally T-7-epitope-tagged yeast NAP1 (49 142 Da) was expressed in *Escherichia coli* strain BL21 (DE3) and purified essentially as described (*11*) with minor modifications (*12*). yNAP1 is >95% pure as judged by SDS−PAGE. yNAP1 concentrations were determined by absorbance using a calculated molar extinction coefficient of 36100 M^{-1} cm^{-1} at 276 nm (*19*).

Gel Electrophoresis. Proteins were dialyzed into 20 mM Tris, pH 7.6 (4 °C), 100 mM NaCl, 1 mM EDTA prior to electrophoresis. Native polyacrylamide gel electrophoresis was carried out as described previously (*12*).

Chemical Cross-Linking. Self-association of yNAP1 was characterized directly by chemical cross-linking using dimethyl suberimidate (*20*, *21*) at a final concentration of 1.0 mg/mL. Prior to cross-linking, yNAP1 was dialyzed extensively against 0.1 M sodium borate, pH 9.0, to remove the inhibitory, amine-rich Tris buffer from the reaction. Protein was incubated at 0.25 mg/mL (5 μM) for the indicated times at 20−22 °C, and aliquots were quenched by the addition of glycine (50 mM final). Samples were dialyzed extensively against 20 mM Tris (pH 7.6, 4 °C), 100 mM NaCl, 1 mM EDTA, and 1 mM DTT, and concentrated in Microcon C-30 microconcentrators (Amicon). Proteins were separated by native PAGE as described above. Native and cross-linked yNAP1 was subject to MALDI-TOF spectrometry with a Voyager DE-Pro mass spectrometer (Perseptive Biosystems) in linear mode.

Gel Filtration Studies. Gel filtration chromatography was performed on an AKTA FPLC using a Superdex S-200 16/60 (120 mL) column (Amersham Biosciences). Following equilibration in either 100 or 500 mM NaCl chromatography buffer, 100−500 μL samples were applied and run at 0.5 mL/min and 5 °C. The retention volumes were calibrated using the gel filtration calibration standard set (Amersham Biosciences). K_{av} for the standards and yNAP1 were determined as described in the calibration kit and plotted versus molecular weight on a logarithmic scale. The resulting equation for the best-fit line was used to determine the apparent molecular weight on the basis of the K_{av} for yNAP1. The Stokes radius of yNAP1 was determined by plotting a standard curve of the K_{av} for the calibration standard set versus the known Stokes radii.

Analytical Ultracentrifugation Studies. AUC experiments were performed with a Beckman XL-I analytical ultracentrifuge using absorbance optics. Velocity measurements utilized a two-sector, charcoal-filled Epon centerpiece, quartz windows, and 400 μL sample and 420 μL reference (buffer) volumes. All samples were centrifuged in a Beckman An60Ti 4-hole rotor at 5 °C. Velocity data were edited and analyzed using the boundary analysis method of van Holde and Weischet as implemented in Ultrascan version 5.0 (*22*). All sedimentation coefficients are reported in units of Svedbergs (S), where $1\ S = 1 \times 10^{-13}$ s, and corrected to that of water at 20 °C (20,W). Modeling of hydrodynamic parameters was performed within Ultrascan.

Equilibrium experiments were performed with a six-sector, charcoal-filled Epon centerpiece using at least three different speeds (14K, 16K, and 18K rpm for the high salt and guanidine conditions, 7−18K rpm for the lower salt conditions). Samples of 100 μL and 110 μL reference (buffer) volumes were used. To account for different loading concentrations while staying within the dynamic range of the detector, absorbance data were collected at 228, 280, and 289 nm. Data were acquired in 0.001 cm increments, and 20−30 measurements were averaged at each radial position. Comparisons of successive scans taken 4−8 h apart confirmed that the samples had reached equilibrium. Equilibrium data were edited and analyzed using self-association models within Origin version 4.1 (Microcal and Beckman) to determine the best fit as evaluated by the distribution of residuals. Global fitting of sedimentation equilibrium data sets was performed within Ultrascan. The partial specific volume ($\bar{v}$, 0.7174 at 5 °C) was calculated from the primary amino acid sequence (*23*), and solvent densities (ρ) were calculated within the Ultrascan software. The apparent isopotential partial specific volume ($\varphi_{2'}$), which compensates for preferential binding of the denaturant to the protein, was calculated for solutions containing guanidine (*24*). However, the value for the 1 M guanidine hydrochloride (GuHCl) solution did not differ significantly from $\bar{v}$ (0.76 vs 0.73 at 22 °C, respectively), and thus had negligible affects on the resulting S(20,W) and mass values.

Solubility/stability assays were performed by incubating 100 μL of 18 μM yNAP1 (A_{276} of 0.66) at 25 combinations of pH values (5.6, 6.6, 7.6, 8.6, and 9.6) and NaCl concentrations (75, 100, 125, 150, and 175 mM). Samples were incubated for 96 h at 5 °C to simulate the length and temperature of a typical sedimentation equilibrium experiment. Samples were then spun at 13K rpm in a refrigerated microcentrifuge, and the A_{276} of the supernatant was measured. Results were recorded as the fraction remaining in solution versus conditions to determine the relative solubility.

Circular Dichroism. CD spectra were collected with a Jasco 720 spectropolarimeter at 5 °C. A total of 20 spectra were obtained and averaged. Samples were dialyzed in 20 mM NaH_2PO_4, pH 7.6, 75 mM NaCl. Measurement of native yNAP1 extended from 260 to 190 nm. Measurements with increasing GuHCl were limited to 260 to 202−205 nm due to high absorbance in the far UV. The molar ellipticity [Θ] was obtained by normalization of the measured ellipticity (Θ, mdeg), using $[\Theta] = (\Theta \times 100)/(nlc)$, where n is the number of residues (430), c is the total concentration (mM), and l is the cell path length (cm) (*25*). The percentage of secondary structure types was determined by an average of the three different analyses contained within the CDPro analytical software (*26*). Analysis of the changes in α-helical content upon addition of denaturant was calculated as described previously (*27*).

RESULTS

yNAP1 Exhibits a Complex Self-Association Behavior. We have previously noted the presence of two yNAP1 species

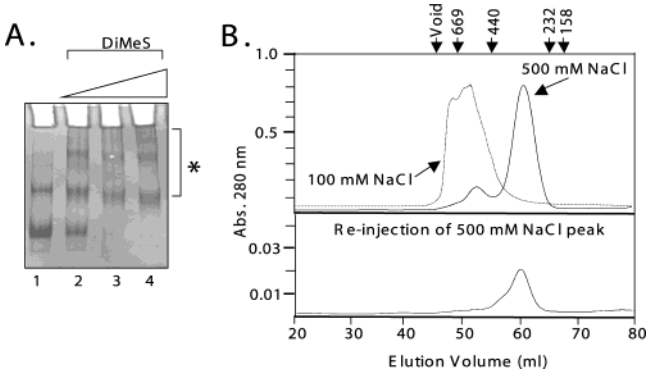

FIGURE 1: Protein cross-linking shows the presence of multiple yNAP1 species. (A) Native PAGE: lane 1, 2.5 μg of yNAP1 in cross-link buffer; lanes 2−4, 15 μg of yNAP1 cross-linked with dimethyl suberimidate (DiMeS; 1 mg/mL) for 15, 60, and 120 min (asterisk indicates cross-linked species). (B) Gel filtration profiles of yNAP1: upper traces, equivalent amounts of yNAP1 were injected in either 100 or 500 mM NaCl and data were recorded at 280 nm; lower trace, 0.1 mL of the peak fraction from separation in 500 mM NaCl (above) was re-injected in 500 mM NaCl. The elution volume is shown (bottom), as is the elution position of the calibration standards (top). Note the different absorbance scales for the upper and lower panels.

upon native gel electrophoresis at 100 mM NaCl (*12*). It appeared that the slower migrating of these species was capable of binding histones, as its mobility was decreased in the presence of the H2A−H2B dimer. To qualitatively assess the oligomeric state of yNAP1 in solution, we carried out chemical cross-linking using dimethyl suberimidate in 100 mM sodium borate and analyzed the products by PAGE. Native gel electrophoresis revealed multiple, distinct species consistent with self-association (Figure 1A). SDS−PAGE revealed a broad, diffuse band centered at 150 kDa (data not shown). The diffuse nature of the band is indicative of the heterogeneity with which cross-linking reagents ligate their substrates. While the apparent molecular weight would suggest the species to be trimeric, the identity remained in doubt because yNAP1 migrates significantly slower (~65 kDa) on SDS−PAGE than expected for a 49 kDa protein, an effect that is likely due to decreased binding of SDS to the highly acidic protein (*28*). Additionally, the neutralization of lysine side chains involved in the cross-linking may affect the migration rate on a gel. Therefore, from these data we were able to conclude that yNAP1 forms oligomers in solution, though an unambiguous identification of the various oligomeric species could not be determined.

To determine the molecular masses of the cross-linked species, we subjected cross-linked yNAP1 to MALDI-TOF spectrometry. The mass spectrum showed defined peaks of masses consistent with yNAP1 monomers and dimers (51 and 102 kDa), while no evidence for larger species was seen (data not shown). The peak of monomeric mass is likely the result of noncovalently cross-linked dimers dissociating under the mass spectrometry conditions. The inability of MALDI-TOF to detect the larger oligomers suggested by native PAGE data (Figure 1A) is likely a consequence of the loss of sensitivity at masses greater than 100 kDa. Taken together, these data suggest that yNAP1 can form dimers and larger oligomers in solution, though the number and composition of the oligomers could not be determined.

The Heterogeneity of yNAP1 Can Be Restricted by Increasing Ionic Strength. To examine the oligomerization of yNAP1 in solution, we analyzed yNAP1 using calibrated GFC at 100 mM NaCl (Figure 1B). The apparent molecular mass values returned by this analysis were 500 kDa to 1 MDa, much larger than the species detectable by mass spectrometry. Interestingly, gel filtration at higher ionic strength (500 mM NaCl) yielded a discrete peak at lower apparent molecular weight (MW_{app}), and re-injection of a portion of this peak showed an identical elution time (Figure 1B). However, the MW_{app} (~300 kDa) and Stokes radius (56 Å) for this peak were much larger than those observed by native PAGE and cross-linking analyses. This showed that larger species present at 100 mM NaCl could be disrupted by 500 mM NaCl and that the resulting MW_{app} is not dependent on protein concentration.

The complexity of yNAP1 self-association and the anomalous results obtained by cross-linking followed by mass spectrometry and by GFC led us to utilize analytical ultracentrifugation to rigorously determine the oligomerization state of yNAP1 in solution. Sedimentation velocity (SV) experiments of yNAP1 were analyzed by the boundary analysis method of van Holde and Weischet (*29*). At 150 mM NaCl, the integral distribution of sedimentation coefficients, $G(s)$, indicated a heterogeneous population of species with sedimentation coefficients from ~5 to ~7 S (Figure 2A). The $G(s)$ plot was consistent with an association/dissociation reaction of moderate affinity occurring on the time scale of the experiment (*22*). In contrast, sedimentation in 500 mM NaCl revealed a single, homogeneous species of approximately 4.5 S, consistent with the salt-dependent dissociation of yNAP1 aggregates seen in GFC experiments at this higher ionic strength (Figure 1B). This conversion appears to be rapid, as a sample equilibrated at the lower salt is converted to the homogeneous 4.5 S species by the addition of NaCl to 500 mM immediately prior to sedimentation (Figure 2A).

To more precisely determine the effects of salt concentration on oligomerization, we carried out SV experiments on yNAP1 at salt concentrations ranging from 10 to 500 mM NaCl and generated a $G(s)$ plot for each salt condition (Figure 2B). The effects due to salt titration are best visualized by plotting the average S values for the upper 10% of each boundary analysis versus NaCl concentration (Figure 2C). This shows that, above ~300 mM NaCl, yNAP1 is a homogeneous population of 4.5 S. However, when the salt concentration is decreased to a more physiologic level (50−150 mM NaCl), the protein self-associates into much larger oligomers, extending to ~12 S. Interestingly, much of this self-association is lost as the salt concentration is decreased further (10−25 mM NaCl). The self-association of yNAP1 also exhibits strong protein concentration dependence at 75 mM NaCl (0.5−25 μM, Figure 2D). Again, high salt concentration (500 mM) eliminated self-association and yielded essentially overlapping ~4.5 S sedimentation values at these same protein concentrations (Figure 2E). Under both salt conditions a small fraction of a more slowly sedimenting material (<4.5 S) was seen at the lowest protein concentration and may be indicative of minor dissociation of the 4.5 S species.

yNAP1 Dimers Self-Associate into Larger Oligomers. We used sedimentation equilibrium to rigorously determine the molecular weight of the homogeneous 4.5 S species and to examine the self-association of yNAP1 at moderate ionic

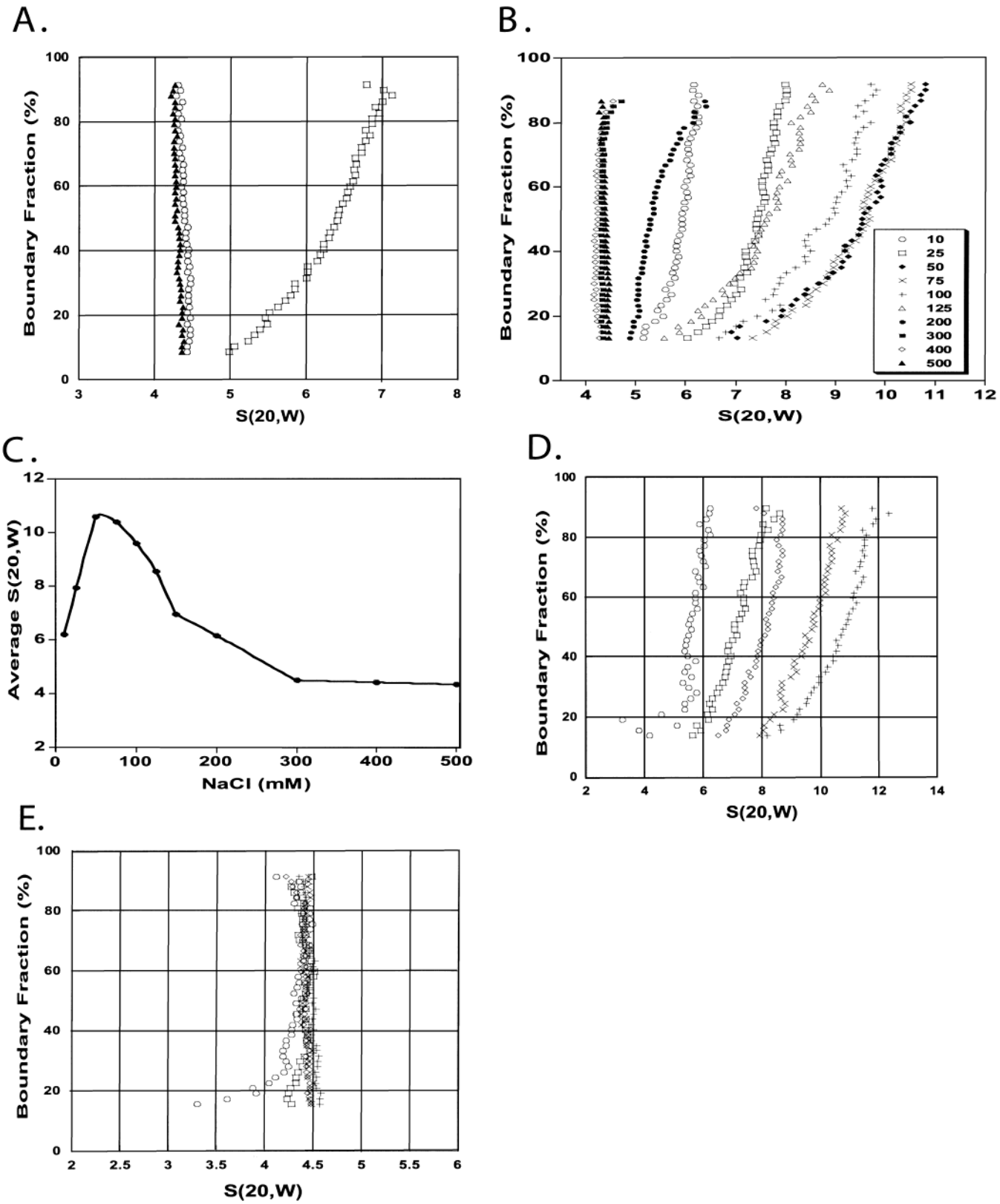

FIGURE 2: (A−C) *G*(*s*) plots of sedimentation velocity data show changes in the oligomerization state of yNAP1 due to changes in ionic strength. (A) *G*(*s*) plots of 11 μM yNAP1at 150 mM NaCl (□) and 500 mM NaCl (○) and a solution dialyzed to 150 mM and then brought to 500 mM immediately prior to sedimentation (▲). (B) *G*(*s*) plot of 11 μM yNAP1 at a range of NaCl concentrations (indicated in the legend, mM). (C) Average S(20,w) obtained from the upper 10% of the boundaries in (B), representing the fastest sedimenting species, as a function of NaCl concentration. (D, E) *G*(*s*) plots of sedimentation velocity data show a loss of higher order oligomers at 500 mM NaCl. *G*(*s*) plots of yNAP1 at 0.5 μM (○), 2 μM (□), 5 μM (◇),10 μM (×), and 25 μM (+) in 75 mM NaCl (D) or 500 mM NaCl (E).

strength. The mass of yNAP1 derived from sedimentation equilibrium at 500 mM NaCl fluctuated near the calculated value of the yNAP1 dimer (98 kDa) (Table 1), regardless of the protein concentration or rotor speed. In contrast, yNAP1 in 75 mM NaCl showed a clear increase in mass as the protein concentration was increased. This is consistent with

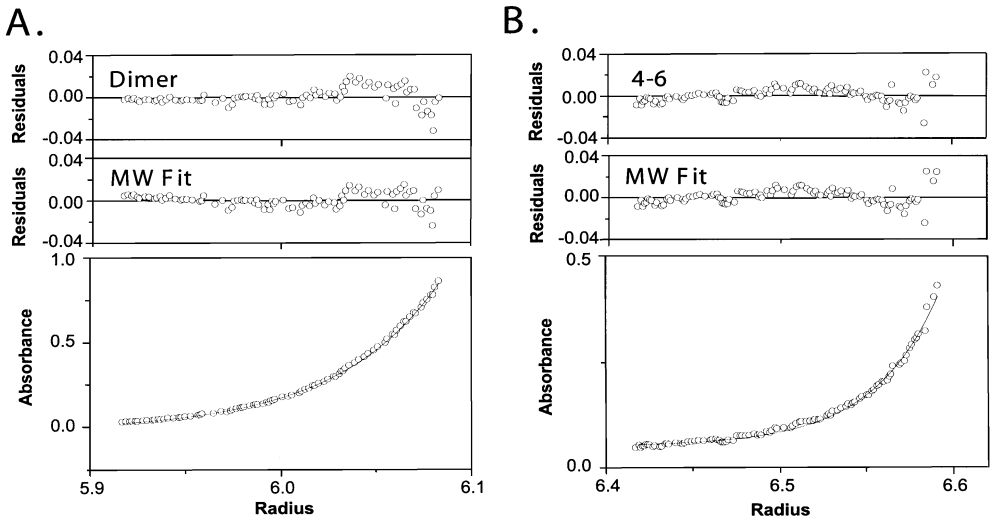

FIGURE 3: (A) Sedimentation equilibrium of yNAP1 (13.8 μM) at high ionic strength (500 mM NaCl) and 16K rpm. The data are well described by an ideal, single species with the mass of a yNAP1 dimer (93 kDa observed vs 98.3 kDa calculated). Note the similarity of the residuals resulting from the two models [fixed molecular weight dimer (rms deviation 0.0067, upper panel), and fitting the molecular weight to the data (rms deviation 0.0066, lower panel)]. (B) Sedimentation equilibrium of yNAP1 (1.4 μM) at 150 mM NaCl and 12K rpm. The mass returned from this analysis (209 kDa) indicates the presence of higher order yNAP1 oligomers. The systematic deviations in the residuals indicate that the tetramer−hexamer model (4−6) does not accurately describe the system.

Table 1: Weight Average Mass by Sedimentation

concn (μM)	[NaCl] (mM)	molecular mass[a] (kDa)	concn (μM)	[NaCl] (mM)	molecular mass[a] (kDa)
0.5	500	82 ± 28	0.5	75	115 ± 9
1.4	500	94 ± 6	1.4	75	141 ± 29
5.5	500	106 ± 1	5.5	75	204 ± 46
14	500	92 ± 2	14	75	248 ± 24
			25	75	263 ± 16
			50	75	239 ± 23
			100	75	257 ± 42

[a] The weight average molecular masses expressed are the average of the values determined for each speed (14, 16, and 18K rpm) with the indicated standard deviation.

a self-association equilibrium obeying the laws of mass action, where higher protein concentration drives the formation of larger oligomers at the expense of smaller species.

Sedimentation equilibrium data of yNAP1 in 500 mM NaCl were best fit to a single ideal component having a mass of 93 kDa (Figure 3). This mass is within 5% of the expected mass of the yNAP1 dimer (98 kDa) and is consistent with SV experiments indicating that the sample is homogeneous at 500 mM NaCl (Figure 2E). The slight systematic deviation in the residuals suggests a monomer−dimer equilibrium, but we were unable to reliably obtain an association constant because the monomeric species was so underrepresented in the population. Thus, under high salt conditions, yNAP1 is best described as a nearly pure solution of yNAP1 dimers.

At 75 mM NaCl, sedimentation equilibrium showed a decrease in sample absorbance as a function of increasing rotor speed, indicating a loss of sample due to pelleting (data not shown). This effect is more pronounced at higher speeds because the protein concentration at the bottom of the cell increases with the higher centrifugal force, driving the equilibrium toward the larger species. A systematic evaluation of the solubility of yNAP1 was performed (see Experimental Procedures) and showed that the solubility of the protein was improved at increased ionic strength (150−175 mM NaCl) and higher pH (8.6) (data not shown). An example of a sedimentation equilibrium gradient obtained under these conditions is shown in Figure 3B. The mass returned by analysis of this gradient (209 kDa) suggests the presence of larger yNAP1 oligomers (tetramers and possibly larger species). However, even under these improved conditions, sedimentation equilibrium gradients revealed evidence of pelleting of a small fraction of the sample even at the low speeds (7−12K rpm) appropriate for resolving potentially large aggregates. This loss of material, though only a small fraction of the sample, prohibited rigorous fitting of the low salt data to self-association models. Nonetheless, we were able to observe a correlation between the loading concentration and the average mass of the species (Table 1). Fitting of the data to a single, ideal species model results in weight average mass values that appear to plateau at 250−300 kDa as concentrations approach 25 μM. However, fitting of the data to a self-association scheme culminating in pentamers or hexamers did not produce statistically reliable results, as indicated by large and systematic deviations in the residuals. Thus, under moderate salt concentrations, yNAP1 self-associates and appears to form large aggregates that pellet during the experiment, precluding a rigorous evaluation of the self-association scheme.

The Extent of yNAP1 Self-Association Can Be Controlled by Moderate Levels of Chaotrope. Even at the lowest concentration of yNAP1 used in the ultracentrifugation experiments (0.5 μM), no significant species smaller than the 4.5 S dimer are seen. To dissociate the 4.5 S/98 kDa yNAP1 dimer, samples of identical protein concentration and increasing concentrations of GuHCl were subjected to sedimentation velocity (Figure 4). van Holde−Weischet analysis of yNAP1 in 75 mM NaCl and 1 M GuHCl led to a $G(s)$ plot nearly identical to that of the monodisperse 4.5 S species seen in 500 mM NaCl in the absence of chaotrope (compare with Figure 2A,E). Thus, either high salt or 1 M GuHCl can abrogate the yNAP1 heterogeneity resulting from higher order oligomerization. At a slightly higher concentration of denaturant, 1.8 M GuHCl, the monodisperse 4.5 S species was converted to a monodisperse 2.4 S species. Determination of the absolute molecular mass of the 2.4 S

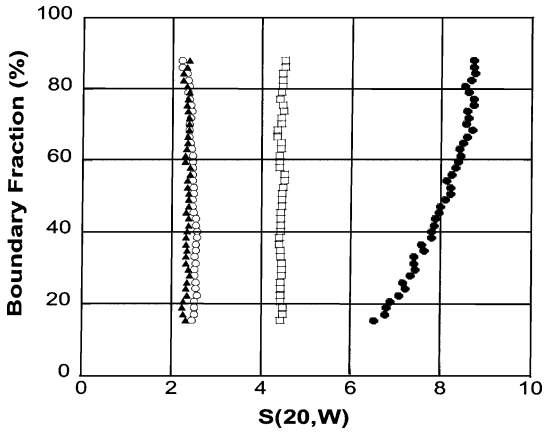

FIGURE 4: *G*(*s*) plots of sedimentation velocity data show sequential dissociation of yNAP1 oligomers in the presence of GuHCl. *G*(*s*) distributions of 5 μM yNAP1 equilibrated at 0.0 M (●), 1.0 M (□), 1.8 M (○), and 2.0 M (▲) GuHCl.

Table 2: Sedimentation Equilibrium Analysis of yNAP1 in GuHCl

GuHCl concn (M)	weight average molecular mass[a] (kDa)	GuHCl concn (M)	weight average molecular mass[a] (kDa)
0.0	226 ± 22	1.5	69 ± 7
1.0	89 ± 7	1.8	48 ± 3

[a] The weight average molecular masses are the average of the values determined for each speed (14, 16, and 18K rpm) with the indicated standard deviation.

species was accomplished by performing sedimentation equilibrium in the presence of chaotrope. This revealed a mass that is nearly identical to the calculated monomer mass (48 vs 49 kDa, Table 2). Taken together with the SV analysis (Figure 4), these data show that the presence of ≥1.8 M GuHCl dissociates the 4.5 S yNAP1 dimers into 2.4 S monomers.

Formation of yNAP1 Monomers Is Accompanied by Loss of Secondary Structure. We used circular dichroism spectroscopy to determine the structural changes associated with the loss of higher order oligomers and the subsequent appearance of the monomer upon addition of GuHCl. CD spectroscopy is highly sensitive to changes in the secondary structure of polypeptides (*30*). The spectrum obtained in 75 mM NaCl (in the absence of chaotrope) was deconvoluted to determine the proportions of secondary structure components (*26*). This analysis revealed that yNAP1 is ∼34% α-helical, ∼33% β-sheet and turn, and ∼33% unstructured. The intensities of peaks within the spectra of yNAP1 undergo only subtle changes at concentrations of GuHCl less than 1.5 M (Figure 5A). However, the CD spectrum of yNAP1 in 1.8 M GuHCl is indicative of a highly unstructured polypeptide, and higher amounts of GuHCl (4 M) lead to a spectrum consistent with a completely denatured polypeptide. The strong absorbance of GuHCl at wavelengths less than 200 nm precluded a rigorous, quantitative analysis of secondary structure in the presence of chaotrope. However, the ellipticity at 222 nm correlates with the proportion of α-helix, and changes in $[\Theta]_{222}$ can be expressed as a loss or gain in α-helical content (*31*). This type of analysis for yNAP1 in the absence of denaturant yielded an α-helical content of ∼31%, similar to that obtained by the more rigorous analysis. Analysis of the intensity at 222 nm for increasing amounts of GuHCl is shown in Figure 5B. The first step, between 0.0 and 1.5 M GuHCl, corresponds to a loss of ∼40% of the helical content of yNAP1 (from 31% to 18%). A much more striking loss of negative ellipticity is seen as GuHCl is further increased to 1.8 M. The slight (0.3 M) increase in chaotrope yields a net loss in α-helical content of 90% (to ∼3%) relative to the native protein. The changes in the CD spectra correlate well with the changes in the sedimentation coefficient and mass observed as a function of GuHCl concentration (Figure 4, Table 2), and indicate that dissociation of the yNAP1 dimer is linked to the formation of an unstructured monomer.

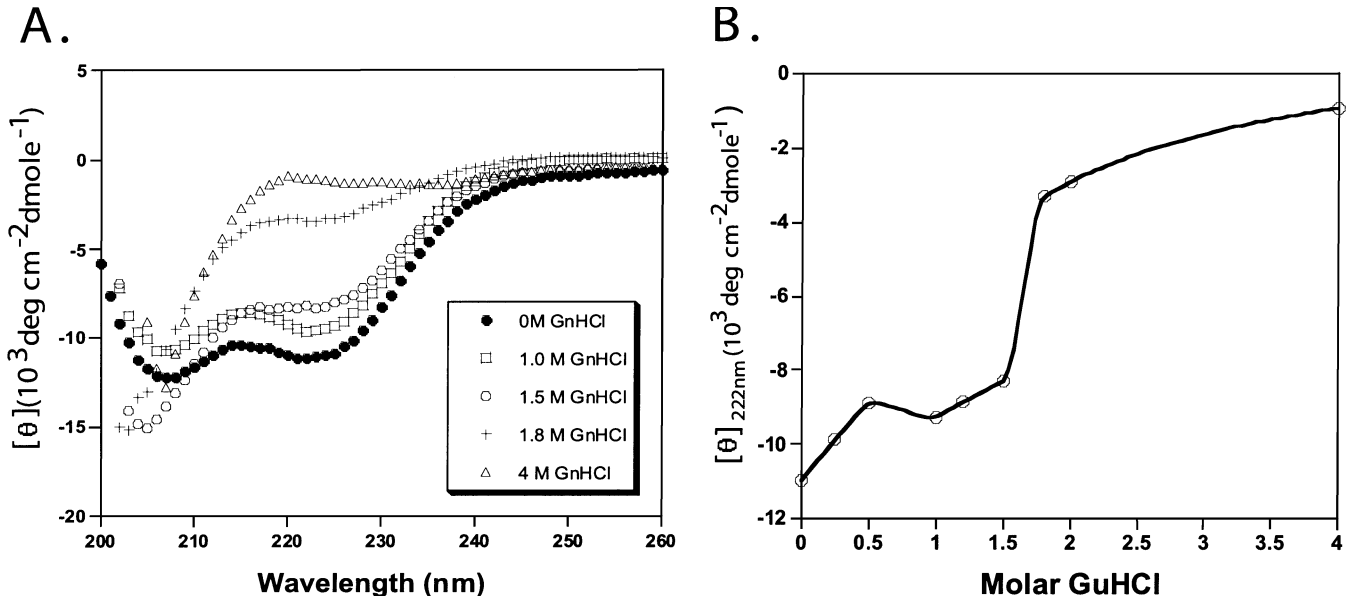

FIGURE 5: CD spectroscopy indicates a three-step loss of secondary structure. (A) 10 μM yNAP1 was equilibrated with 0.0, 0.25, 0.5,1.0, 1.2, 1.5, 1.8, and 4.0 M GuHCl in 75 mM NaCl. CD spectra were collected at 5 °C, and the CD signal was normalized on a per-residue basis (for clarity, not all spectra are shown). (B) Changes in the CD signal at 222 nm as a function of GuHCl concentration from data collected in (A). $[\Theta]_{222nm}$ is normalized on a per-residue basis, and a smooth curve fit of the data is shown.

DISCUSSION

We have defined the self-association behavior of a chromatin assembly factor which is an important biochemical tool used in the study of chromatin organization and dynamics. The results of our biochemical and biophysical studies demonstrate that the fundamental oligomerization state of yNAP1 is a stable dimer and that this dimer self-associates under physiological salt concentrations. Our observations further support the idea that self-association is a general property of histone chaperone proteins.

Gel filtration data indicate that the 98 kDa yNAP1 dimers in 500 mM NaCl elute at an anomalously high apparent molecular mass of ~300 kDa and with a Stokes radius of 56 Å, significantly larger than the ~30 Å radius expected for a spherical protein. Similarly, modeling of the shape of yNAP1 based on its sedimentation rate showed that the 4.5 S dimer could be modeled as an ellipsoid with an axial ratio of approximately 1.8. A previous study utilizing limited proteolysis and CD spectroscopy revealed that yNAP1 has a protease-sensitive N-terminus, a well-structured central region (aa 74−365), and a C-terminal (aa 365−417) histone-binding domain that is largely devoid of secondary structure (*12*). The overall elongated or extended shape of yNAP1 suggested by its hydrodynamic properties could result from such a modular structure combined with the preponderance of unstructured amino acids (~33%).

Oligomerization of the 4.5 S dimer can be abrogated by the presence of high ionic strength, resulting in a relatively homogeneous distribution of species regardless of protein concentration. Further, sedimentation equilibrium of yNAP1 in high salt over a 50-fold range in protein concentration led to weight average molecular masses of 82−106 kDa (mean 93.4), within experimental error for a 98 kDa yNAP1 dimer. Interestingly, the loss of heterogeneity seen at high salt (≥300 mM) is also seen, to a lesser extent, at very low salt (≤10 mM) (see Figure 2B,C). It is likely that high ionic strength disrupts intermolecular hydrogen bonds and salt bridges, while low ionic strength leads to charge repulsion between the highly negatively charged yNAP1 dimers. Both these phenomena lead to a loss of higher order oligomerization. Consistent with these hypotheses, permanent protein−protein interfaces such as those found in homodimers are generally rich in hydrophobic side chains (*32*), and contain few, if any, salt bridges (*33*). These interfaces are thus less sensitive to disruption by increased ionic strength. However, the side chains found at the protein−protein interface of "nonobligate" (higher order) complexes are more likely polar in nature, and are thus more easily disrupted by ionic strength (*33*). It is reasonable to conclude, therefore, that formation of higher order oligomers due to electrostatic interactions would be readily abrogated by high salt. This appears to be the case for yNAP1.

The determination of the hetero- or homogeneity of the samples using sedimentation velocity experiments allowed for informed application of sedimentation equilibrium-derived self-association models. Self-association of yNAP1 is best described as a rapid, concentration-dependent assembly of stable dimers into larger oligomers. We stipulate, however, that thermodynamic nonideality due to the high yNAP1 concentration (25−100 μM) could have led to an underestimation of the mass of the largest species in this associative reaction (*34*). The sample loss we observed in sedimentation equilibrium experiments is likely the result of pelleting of oligomers larger than the observed apparent maximal hexameric stoichiometry (~300 kDa) (Table 1).

The apparent three-state denaturation of yNAP1 by GuHCl titration likely involves two separate molecular events. The first is a loss of intermolecular contacts between higher order yNAP1 oligomers that occurs at ~1.0 M GuHCl and yields a monodisperse population of dimers. This requires only a minimal change in secondary structure. Thus, the loss of higher order oligomers requires sufficient ionic strength (or desolvation) provided by the salt (or chaotrope) to abrogate the intermolecular electrostatic attractions between dimers. At ≥1.8 M GuHCl, a homogeneous population of 2.4 S species is observed, and this conversion is concomitant with a large change in the CD spectrum showing that nearly complete denaturation of yNAP1 accompanies the dissociation of the 4.5 S dimer. These higher denaturant amounts likely preclude formation of the secondary structure required for yNAP1 dimerization. The CD spectra show a clear loss of the 208 and 222 nm minima during denaturation, suggesting that an α-helical structure may be involved in the dimerization interface. A survey of the secondary structure content of 28 homodimeric proteins revealed that over half (53%) of the interface residues were classified as α-helix (*32*).

Histone fold domains generally show little similarity with regard to their amino acid sequence, although their overall amino acid content (*35*) and secondary structure (*36*) are extremely well conserved. Each pair of histone molecules associate through antiparallel contacts between the longest helices (α2) of the canonical histone fold motif (*36*). In solution, two H3−H4 dimers are linked through the formation of a four-helix bundle between the second of two helix−strand−helix motifs in H3 (*4*, *36*). As a result, the tertiary structures of the H2A−H2B dimer and half of the $(H3-H4)_2$ tetramer are essentially superimposable (*1*, *4*, *35*). In each of these complexes, two essentially identical surfaces are solvent exposed per pair of histone folds. The stoichiometries of yNAP1−histone complexes have been demonstrated to be two yNAP1 molecules per histone dimer and four per histone tetramer (*10*, *12*, *13*). Our data show that the fundamental oligomerization state of yNAP1 is a dimer, suggesting that each yNAP1 dimer binds one histone dimer and that two yNAP1 dimers bind the $(H3-H4)_2$ tetramer.

The specific geometry of the yNAP1 dimer and its complexes with histone dimers is not yet known. We envision two possible models for how yNAP1 binds histone dimers. In our first model, the yNAP1 dimer straddles the edge of the roughly planar histone dimer such that the two yNAP1 monomers interact with opposite faces of the histone dimer in a clamping fashion. In this complex, both surfaces of the histone dimer may be effectively shielded from interactions with other proteins. In the second model, the yNAP1 dimer interacts with just one face of the histone dimer and the other face remains solvent exposed and can interact with other proteins. In either model, the central structured portion of yNAP1 (residues 74−365 (*12*)) likely forms the core of the yNAP1 dimer interaction. The antiparallel symmetry of the histone dimers may argue that this orientation is also the logical arrangement for the yNAP1 dimer, but the orientation is not yet known.

Last, we can only speculate about the role of higher order yNAP1 oligomers in histone binding and nucleosome assembly. Though no quantitative measurements of yNAP1 concentrations in vivo have been reported, it is possible that local concentrations within the nucleus allow for some degree of self-association. Perhaps the aggregates we observe at physiologic salt concentrations represent a storage form of unliganded yNAP1. Further, binding to the highly charged and basic histones may abolish the higher order oligomerization of yNAP1 dimers and result in the formation of discrete yNAP1 dimer−histone dimer complexes in solution, analogous to the deaggregation we observe at high salt concentrations. Elucidation of these details will require further study of yNAP1−histone complexes and their stoichiometries and oligomerization potential.

ACKNOWLEDGMENT

We gratefully acknowledge Jeffrey Hansen for helpful discussions and assistance in preparation of the manuscript. We also thank Borries Demeler for help in the use of his analysis software.

REFERENCES

1. Arents, G., Burlingame, R. W., Wang, B. C., Love, W. E., and Moudrianakis, E. N. (1991) The nucleosomal core histone octamer at 3.1 A resolution: a tripartite protein assembly and a left-handed superhelix, *Proc. Natl. Acad. Sci. U.S.A. 88*, 10148−10152.
2. Richmond, T. J., Finch, J. T., Rushton, B., Rhodes, D., and Klug, A. (1984) Structure of the nucleosome core particle at 7 A resolution, *Nature 311*, 532−537.
3. Akey, C. W., and Luger, K. (2003) Histone chaperones and nucleosome assembly, *Curr. Opin. Struct. Biol. 13*, 6−14.
4. Luger, K., Mader, A. W., Richmond, R. K., Sargent, D. F., and Richmond, T. J. (1997) Crystal structure of the nucleosome core particle at 2.8 A resolution, *Nature 389*, 251−260.
5. Kimura, H., and Cook, P. R. (2001) Kinetics of core histones in living human cells: little exchange of H3 and H4 and some rapid exchange of H2B, *J. Cell Biol. 153*, 1341−1353.
6. Krude, T., and Keller, C. (2001) Chromatin assembly during S phase: contributions from histone deposition, DNA replication and the cell division cycle, *Cell Mol. Life Sci. 58*, 665−672.
7. Tyler, J. K. (2002) Chromatin assembly. Cooperation between histone chaperones and ATP-dependent nucleosome remodeling machines, *Eur. J. Biochem. 269*, 2268−2274.
8. Philpott, A., Krude, T., and Laskey, R. A. (2000) Nuclear chaperones, *Semin. Cell Dev. Biol. 11*, 7−14.
9. Ito, T., Bulger, M., Kobayashi, R., and Kadonaga, J. T. (1996) Drosophila NAP-1 is a core histone chaperone that functions in ATP-facilitated assembly of regularly spaced nucleosomal arrays, *Mol. Cell Biol. 16*, 3112−3124.
10. Nakagawa, T., Bulger, M., Muramatsu, M., and Ito, T. (2001) Multistep chromatin assembly on supercoiled plasmid DNA by nucleosome assembly protein-1 and ATP-utilizing chromatin assembly and remodeling factor, *J. Biol. Chem. 276*, 27384−27391.
11. Fujii-Nakata, T., Ishimi, Y., Okuda, A., and Kikuchi, A. (1992) Functional analysis of nucleosome assembly protein, NAP-1. The negatively charged COOH-terminal region is not necessary for the intrinsic assembly activity, *J. Biol. Chem. 267*, 20980−20986.
12. McBryant, S. J., Park, Y. J., Abernathy, S. M., Park, Y. J., Laybourn, P. J., Nyborg, J. K., and K. L. Luger. (2003) Preferential binding of the histone (H3−H4)2 tetramer by NAP1 is mediated by the amino terminal histone tails, *J. Biol. Chem. 278*, 44574−44583.
13. McQuibban, G. A., Commisso-Cappelli, C. N., and Lewis, P. N. (1998) Assembly, remodeling, and histone binding capabilities of yeast nucleosome assembly protein 1, *J. Biol. Chem. 273*, 6582−6590.
14. Ito, T., Ikehara, T., Nakagawa, T., Kraus, W. L., and Muramatsu, M. (2000) p300-mediated acetylation facilitates the transfer of histone H2A−H2B dimers from nucleosomes to a histone chaperone, *Genes Dev. 14*, 1899−1907.
15. Dutta, S., Akey, I. V., Dingwall, C., Hartman, K. L., Laue, T., Nolte, R. T., Head, J. F., and Akey, C. W. (2001) The crystal structure of nucleoplasmin-core: implications for histone binding and nucleosome assembly, *Mol. Cell 8*, 841−853.
16. Namboodiri, V. M., Dutta, S., Akey, I. V., Head, J. F., and Akey, C. W. (2003) The Crystal Structure of Drosophila NLP-Core Provides Insight into Pentamer Formation and Histone Binding, *Structure (London) 11*, 175−186.
17. Arnan, C., Saperas, N., Prieto, C., Chiva, M., and Juan Ausio. (2003) Interaction of nucleoplasmin with core histones, *J. Biol. Chem. 278*, 31319−31324.
18. Dyer, P. N., Edayathumangalam, R. S., White, C. L., Bao, Y., Chakravarthy, S., Muthurajan, U. M., and Luger, K. (2004) Methods for reconstitution of nucleosomes from core histones and DNA, *Methods Enzymol.* (in press).
19. Edelhoch, H. (1967) Spectroscopic determination of tryptophan and tyrosine in proteins, *Biochemistry 6*, 1948−54.
20. Davies, G. E., and Stark, G. R. (1970) Use of dimethyl suberimidate, a cross-linking reagent, in studying the subunit structure of oligomeric proteins, *Proc. Natl. Acad. Sci. U.S.A. 66*, 651−656.
21. Thomas, J. O., and Kornberg, R. D. (1978) The study of histone−histone associations by chemical cross-linking, *Methods Cell Biol. 18*, 429−40.
22. Demeler, B., Saber, H., and Hansen, J. C. (1997) Identification and interpretation of complexity in sedimentation velocity boundaries, *Biophys. J. 72*, 397−407.
23. Perkins, S. J. (1986) Protein volumes and hydration effects. The calculations of partial specific volumes, neutron scattering matchpoints and 280-nm absorption coefficients for proteins and glycoproteins from amino acid sequences, *Eur. J. Biochem. 157*, 169−80.
24. Durchschlag, H., and Jaenicke, R. (1982) Partial specific volume changes of proteins densimetric studies, *Biochem. Biophys. Res. Commun. 108*, 1074−9.
25. Adler, A. J., Greenfield, N. J., and Fasman, G. D. (1973) Circular dichroism and optical rotatory dispersion of proteins and polypeptides, *Methods Enzymol. 27*, 675−735.
26. Sreerama, N., and Woody, R. W. (2000) Estimation of protein secondary structure from circular dichroism spectra: comparison of CONTIN, SELCON, and CDSSTR methods with an expanded reference set, *Anal. Biochem. 287*, 252−260.
27. Chen, Y. H., Yang, J. T., and Martinez, H. M. (1972) Determination of the secondary structures of proteins by circular dichroism and optical rotatory dispersion, *Biochemistry 11*, 4120−4131.
28. Hames, B. D. (1998) *Gel Electrophoresis of Proteins: A Practical Approach*, 3rd ed., pp 13−33, Oxford University Press, Oxford.
29. van Holde, K. E., and (1978) Boundary analysis of sedimentation-velocity experiments with mondisperse and paucidisperse solutes, *Biopolymers 17*, 1387−1403.
30. Berova, N., Nakanishi, K., and Woody, R. W. (2000) *Circular Dichroism: Principles and Applications*, Wiley-VCH Inc., New York.
31. Fasman, G. D. (1996) *Circular dichroism and the conformational analysis of biomolecules*, Plenum Press, New York.
32. Jones, S., and Thornton, J. M. (1996) Principles of protein−protein interactions, *Proc. Natl. Acad. Sci. U.S.A. 93*, 13−20.
33. Kleanthous, C. (2000) *Protein−protein recognition*, Oxford University Press, New York.
34. Harding, S. E., Rowe, A. J., and J. Horton. (1992) *Analytical ultracentrifugation in biochemistry and polymer science*, The Royal Society for Chemistry, London, England.
35. Sullivan, S., Sink, D. W., Trout, K. L., Makalowska, I., Taylor, P. M., Baxevanis, A. D., and Landsman, D. (2002) The Histone Database, *Nucleic Acids Res. 30*, 341−2.
36. Arents, G., and Moudrianakis, E. N. (1995) The histone fold: a ubiquitous architectural motif utilized in DNA compaction and protein dimerization, *Proc. Natl. Acad. Sci. U.S.A. 92*, 11170−11174.

BI035881B